Progress In Electromagnetics Research C, Vol. 83, 71–82, 2018

Miniaturized Multiband Microstrip Patch Antenna Using Metamaterial Loading for Wireless Application

Amit K. Singh*, Mahesh P. Abegaonkar, and Shiban K. Koul

Abstract—A highly miniaturized significant gain triple band patch antenna loaded with a new modified double circular slot ring resonator (MDCsRR) metamaterial unit cell is presented in this paper. New MDCsRR is a compact low frequency slot ring resonator. The principle of the proposed patch antenna element is based on adding series capacitance to decrease the half wavelength resonance frequency, thus reducing the electrical size of the proposed patch antenna. The transmission line model is used to analyze passband and stopband characteristics of the radiating bands. Circulating current distribution around MDCsRR slot with increased interdigital capacitor finger length causes multiple modes to propagate. The MDCsRR metamaterial unit cell consists of a new modified circular slot ring resonator (MCsRR) with metallic strip finger. The proposed structure is compact in size with radiating element dimensions of $0.20\lambda \times 0.20\lambda \times 0.008\lambda$ at first resonating frequency. The proposed antenna offers triple band operation with significant calculated antenna gain of 3.28 dBi at first center frequency of 3.2 GHz, 2.76 dBi at second center frequency of 5.4 GHz and 3.1 dBi at third center frequency of 5.8 GHz. The electrical size of the proposed antenna is miniaturized by about 68.83% as compared to the conventional patch antenna operating at first resonating frequency.

1. INTRODUCTION

The next generation RF and microwave devices require two essential characteristics which open possibilities of designing highly integrated microwave circuits. The first one is miniaturization, and the second one is multiband operations with significant gain. Metamaterials are artificial periodic structures having sub-wavelength constituent elements, making the structure behave as a medium with permittivity (ε_r) and permeability (μ) having negative values, not existing in nature. These structures play an important role in designing highly integrated miniaturized multi-band microwave circuits.

Metamaterial unit cell has been used in leaky wave antennas and resonant antennas [1]. Miniaturization of microstrip patch antenna by using metamaterial unit cell has been proposed in [2–4]. Xie et al. [5] has proposed a miniaturized dual band patch antenna where complementary split ring resonator (CSRR) was etched in the ground plane. Ha et al. [6] has presented miniaturization of a patch antenna by using inter digital capacitor (IDC) and CSRR. The multiband microwave antennas are of great interest due to technological advancement in communication systems. Antoniades and Eleftheriades [7] achieved broad band dual-mode operation of a patch antenna by loading with metamaterial transmission line. A multi-band omnidirectional microstrip patch antenna loaded with composite closed-ring resonator and split-ring resonator having CPW feed is reported in [8]. Various other types of multi-band microstrip patch antennas are reported in [9, 10]. A multi-band resonant dipole antenna loaded with metamaterial transmission line is presented by Antoniades and Eleftheriades in [11]. A multi-band antenna with design validation approach is also reported in [12, 13]. Miniaturization of patch antenna is achieved by folding patch and IDC slot with dual-band operation in [14]. A double

Received 29 January 2018, Accepted 20 March 2018, Scheduled 9 April 2018
* Corresponding author: Amit Kumar Singh (amitkumarcareiitd@gmail.com).
The authors are with the Centre for Applied Research in Electronics, Indian Institute of Technology, Delhi 110016, India.

band miniaturized patch antenna using metamaterial unit cell is presented in [15] and triple band miniaturized antenna in [17, 18]. Miniaturization of single to multi-band antennas by using various techniques as slotting metamaterial in ground plane and loading with unit cell is proposed in [19–23] for antenna bandwidth improvements as well as radiation characteristic improvement.

In this paper, a low cost, low profile, highly miniaturized, significant gain triple band patch antenna with good impedance match, loaded with a new modified double circular slot ring resonator (MDCsRR) metamaterial unit cell is presented. New MDCsRR is a compact low frequency slot ring resonator with extended metallic strip fingers. MDCsRR is excited by electric field polarized along the axis of slot ring. The proposed microstrip patch antenna is loaded in series with interdigital capacitor to reduce resonating frequency. To generate multi-mode operation, the proposed patch antenna is further loaded with a new low frequency compact metamaterial unit cell MDCsRR. IDC loaded patch antenna and MDCsRR in ground plane are coupled to generate desired antenna characteristics. Transmission line model is used to analyze passband and stopband characteristics of the resonating bands. Simulated surface current distributions on patch antenna, IDC and MDCsRR are analyzed, and cause of resonant bands is validated by fundamental relations. The proposed antenna is fabricated and extensively characterized. Radiation pattern of the antenna is measured in an anechoic chamber, and excellent isolation between co- and cross-polarized E and H plane is obtained.

2. ANTENNA DESIGN

In this section, antenna design steps are explained. All the design simulations are done using CST microwave studio software. Initially a microstrip patch antenna of dimension 19 mm × 19 mm is designed on Neltec substrate with permittivity (ε_r) = 2.2 and thickness 0.762 mm as shown in Figure 1(a) with simple metallic ground. The antenna resonates at 10.15 GHz (curve "a" of Figure 2). To reduce resonant frequency "f_o" patch antenna is further loaded by interdigital capacitor with simple ground (Figure 1(b)). The resonant frequency is reduced to 7.57 GHz (curve "b" of Figure 2). To reduce

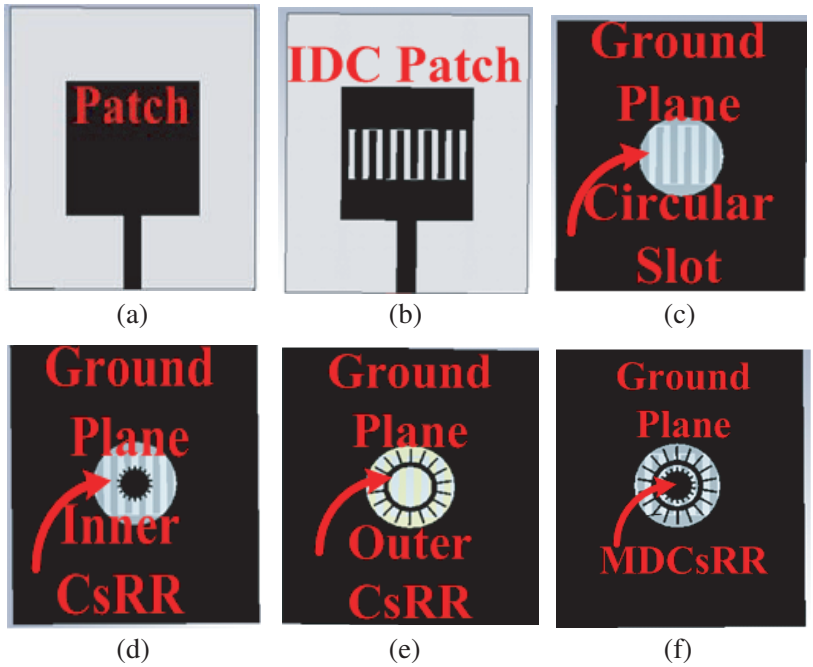

Figure 1. Design steps of proposed antenna loaded with metamaterial unit cell. (a) Square patch antenna with simple ground plane. (b) IDC loaded square patch antenna with simple ground plane. (c) IDC loaded square patch antenna with circular slot in the ground plane. (d) IDC loaded square patch antenna with inner slot ring in the ground plane. (e) IDC loaded patch antenna with outer slot ring only in the ground plane and (f) IDC loaded patch antenna with MDCsRR in the ground plane.

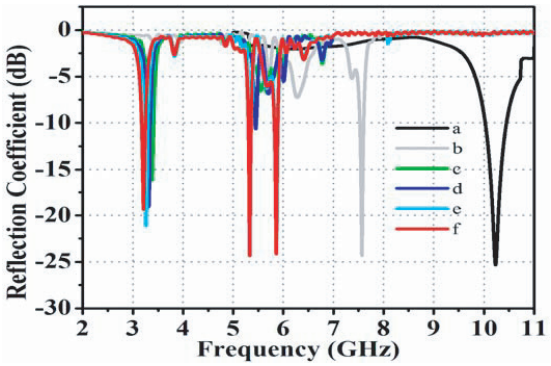

Figure 2. Reflection coefficient (S_{11}) for different proposed antenna structures a, b, c, d, e and f.

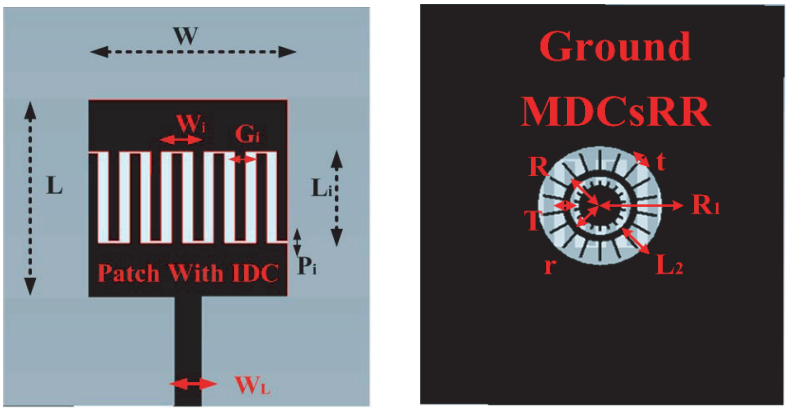

(a) (b)

Figure 3. Proposed metamaterial unit cell loaded microstrip patch antenna. (a) Top view. (b) Back view.

resonating frequency "f_o" further, patch antenna with IDC is loaded with a circular defect of radius $R_1 = 6.00$ mm in ground plane (Figure 1(c)). This causes a major shift in the resonant frequency to 3.39 GHz (curve "c" of Figure 2).To generate second resonating band, the structure of Figure 1(c) is modified to include inner circular slot ring resonator (CsRR) (Figure 1(d)). We observe the first band at 3.31 GHz and second band at 5.45 GHz as shown in Figure 2 (curve "d"). When the combination of patch antenna (Figure 1(b)) and ground plane structure (Figure 1(c)) is further loaded with outer CsRR only (Figure 1(e)), we observe the first band at 3.31 GHz and the second band at 5.85 GHz (Figure 2 curve (e)). The above geometry loaded with modified double circular slot ring resonator (MDCsRR) as shown in Figure 1(f), generates triple band operation. Square patch antenna loaded with IDC and MDCsRR generates three resonant bands with resonating frequency at 3.20 GHz, 5.40 GHz and 5.80 GHz respectively as depicted in Figure 2 (curve "f"). In Figure 1 black color represents metallic section of the proposed design. The loading of patch antenna with IDC and MDCsRR causes major shift in resonant frequency from 10.15 GHz to 3.20 GHz resulting in miniaturization of 68.83% as compared to a conventional patch antenna size (31.25 mm × 37.05 mm × 0.762 mm) operating at 3.20 GHz.

The change in resonant frequency of IDC loaded patch antenna with ground slotting depends on mutual coupling between IDC and the slotted MDCsRR geometry. The prototype microstrip patch antenna loaded with new modified double circular slot ring resonator (MDCsRR) metamaterial unit cell is shown in Figure 3. Table 1 shows various dimensions of the antenna structure.

IDC is a capacitive load added in series with patch antenna equivalent circuit where capacitance due to IDC "C_i" depends on finger length "L_i", finger width "G_i" and air gap "P_i". MDCsRR is a compact low frequency circular slot ring resonator. The detailed circuit model of MDCsRR is given in

Table 1. Design parameters of proposed antenna.

Parameters	Value (mm)	Parameters	Value (mm)
L	19.00	R	3.52
W	19.00	r	1.98
L_i	8.60	R_1	6.00
W_i	3.00	L_1	0.50
G_i	1.00	L_2	1.94
P_i	0.25	T	0.52
W_l	2.76	t	0.20

Figure 4(a), which consists of several capacitances and inductances. Inner ring resonator has equivalent inductance "L_i" due to inner metallic slot and inner ring; "C_{s1}" capacitance is due to inner metallic slot of length "L_1" and outer ring conductor; "C_{r1}" capacitance is due to inner ring and outer ring conductor only; "C_{L1}" is mutual capacitance due to inner metallic fingers only. Outer ring resonator has equivalent inductance "L_o" due to outer metallic slot and outer ring; "C_{s2}" capacitance is due to outer metallic slot of length "L_2" and ground plane; "C_{r2}" capacitance is due to outer ring and ground plane only; "C_{L2}" mutual capacitance is due to outer metallic fingers only. The equivalent circuit model of patch antenna loaded with IDC and MDCsRR consist of LC series tank circuit and shunt LC tank circuit separated by capacitance due to ground "C_g"as shown in Figure 4(b). The shunt LC tank circuit consists of one series combination of "L_o" and "C_2" where "C_2" is the total equivalent capacitance due to outer slot ring resonator. Another shunt LC tank circuit consists of series combination of "L_i" and "C_1" where "C_1" is the total equivalent capacitance due to inner slot ring resonator. Series LC tank circuit consists of series combination of "L_t" and "C_i" where "L_t" is the inductance due to pre-section of transmission line. The shunt capacitance "C_c" is capacitance due to a metallic disc of radius "$r - \frac{c}{2}$" surrounded by a ground plane at a distance of "c" from its edge as given in [3]. The equivalent circuit in Figure 4(b) is obtained by combining equivalent circuit due to IDC, MDCsRR and patch antenna. The circuit parameters are calculated by using conventional analytical approach as given in [16]. The full wave EM simulation of complete structure using CST microwave studio and circuit simulation by using ADS are compared in Figure 5. A small mismatch of about 110 MHz, 30 MHz and 80 MHz at first, second and third resonant frequencies, respectively, is obtained.

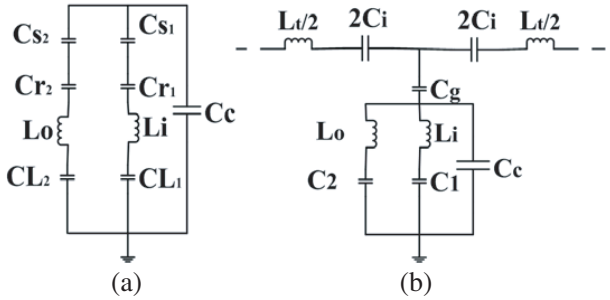

Figure 4. Equivalent circuit of (a) MDCsRR, (b) patch antenna loaded with IDC and MDCsRR.

The source of each capacitance and inductance in the equivalent circuit is identified. The same values can be calculated by using fundamental relations as given in [16]. The inter digital capacitance "C_i" can be calculated by using below equation as shown in [16]

$$C_i = \frac{\varepsilon_{re} 10^{-3}}{18\pi} \frac{K(k)}{K'(k)} (N-1)l \tag{1}$$

The calculated inter digital capacitance is $C_i = 38\,\text{pF}$.

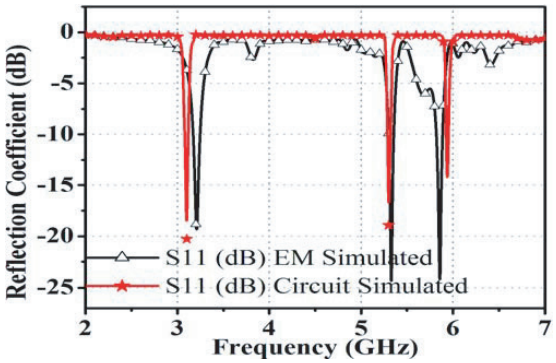

Figure 5. Comparison of circuit and EM simulated reflection coefficients.

The self inductance L of a rectangular strip of length 'l', width 'w' and thickness 't' is given by

$$L = 2 \times 10^{-4} l \left[\ln \left(\frac{l}{w+t} \right) + 1.193 + 0.2235 \frac{w+t}{l} \right] \tag{2}$$

Total self inductance (L_s) is the sum of self inductance of each section.

$$L_s = \sum_{i=1}^{2N-1} L_i \tag{3}$$

The calculated inductance $L_o = 24.5\,\text{nH}$, $L_i = 3.5\,\text{nH}$ and $L_t = 12.5\,\text{nH}$. The capacitances C_g and C_c are calculated by using [6, 7]. The calculated values are $C_g = 92.5\,\text{pF}$ and $C_c = 48\,\text{pF}$. All other capacitances are calculated by using [16] and ADS software optimization tool. The equivalent capacitance $C_1 = 400\,\text{nF}$ and $C_2 = 170\,\text{nF}$.

The geometry of MDCsRR is optimized to get appropriate antenna characteristics. MDCsRR is excited by electric field polarized along the axis of ring and made to resonate at a frequency determined by equivalent capacitance "C_{eq}" and equivalent inductance "L_{eq}" of the modified ring structure. The resonant frequency of MDCsRR is given by $f_o = 1/2\Pi\sqrt{L_{eq}C_{eq}}$, where "$C_{eq}$" is the total equivalent capacitance, and "L_{eq}" is the total equivalent inductance due to MDCsRR. By changing ring parameters equivalent inductance and capacitance can be changed, and MDCsRR can be made to resonate at desired frequency. The proposed MDCsRR unit cell is simulated by using CST microwave studio with appropriate boundary condition, and simulated return loss and transmission characteristic are plotted in Figure 6. It is observed that MDCsRR resonates at two frequencies.

The electric field due to dominant mode propagation within patch cavity is polarized normal to the ground plane. When modified ring resonator is placed in a time varying normal magnetic field, then an electric field will be induced on the metal with a maximum peak value at the resonant frequency.

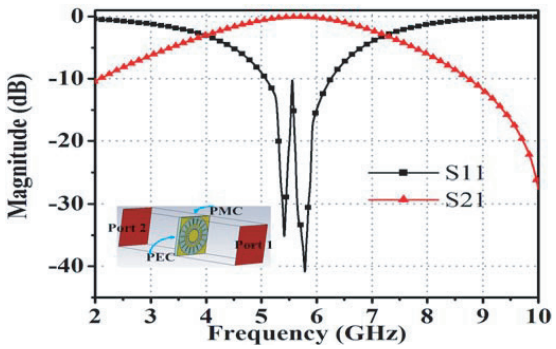

Figure 6. Simulated return loss and transmission parameter of MDCsRR.

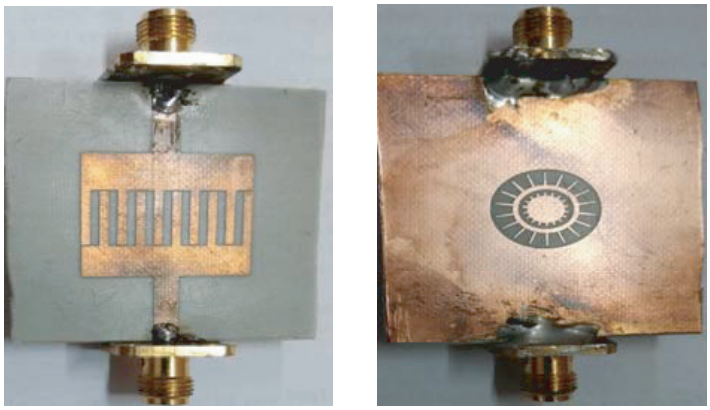

(a) (b)

Figure 7. Fabricated prototype of IDC and MDCsRR loaded transmission line. (a) Top view and (b) back view.

The patch antenna loaded with IDC and MDCsRR is analyzed to study its transmission and reflection characteristics. The transmission line model of proposed patch antenna is derived as reported in [6]. The same model is simulated using high frequency structure simulator CST, and fabricated prototype is shown in Figure 7(a) and Figure 7(b).

Simulated and measured reflection losses and transmission characteristics of designed transmission line model are compared in Figure 8(a) and Figure 8(b), respectively, which show good agreement. A small mismatch in measured and simulated result is due to small fabrication error. The transmission and reflection parameters predict a band-pass filter characteristic at resonating bands of the proposed antenna. The passbands with nearly zero reflection indicate that about zero shunt admittance and matching of antenna in these bands can thus be possible. In stopbands with zero transmission, matching is not possible due to infinite shunt admittance, and hence antenna will not radiate. The simulated surface current distributions are plotted at resonant sample frequencies in Figure 9. Strong surface current concentration can be observed at IDC and MDCsRR.

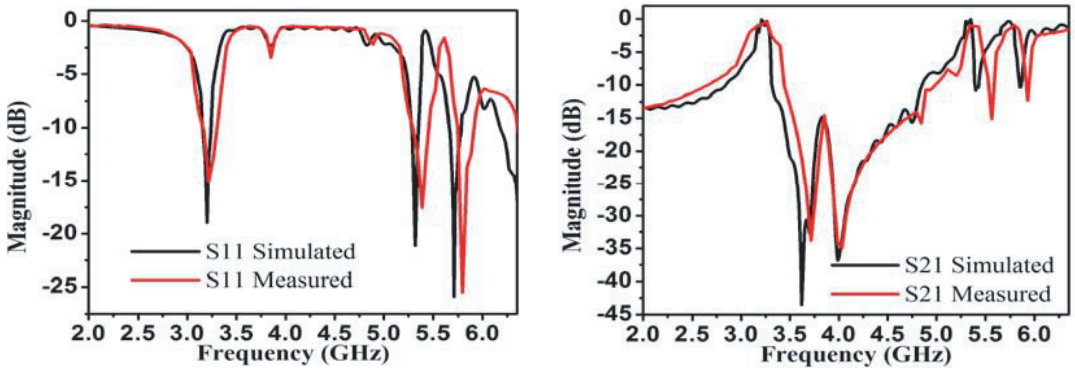

Figure 8. (a) Reflection characteristics and (b) transmission characteristics of proposed IDC and MDCsRR loaded transmission line.

The resonant surface current distribution length is used to validate design strategy for the excitation of triple band as reported in [13]. The same method is applied to validate design strategy of the proposed prototype antenna. The resonating lengths can be calculated by using [12] as

$$f_r = \frac{c}{2L_r\sqrt{\varepsilon_{eff}}} \tag{4}$$

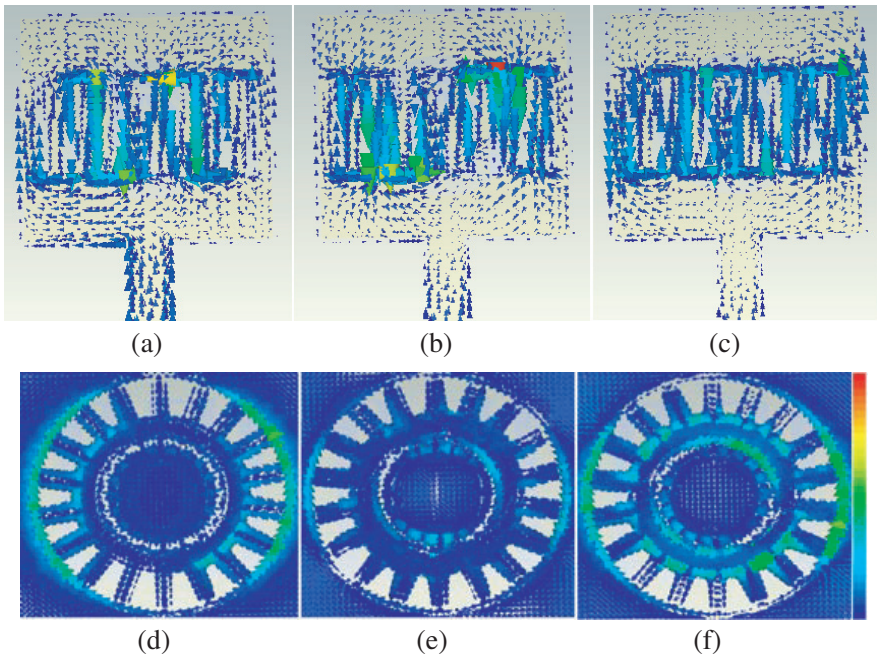

Figure 9. Surface current distribution on (a) patch at 3.2 GHz, (b) patch at 5.4 GHz, (c) patch at 5.8 GHz, (d) MDCsRR at 3.2 GHz, (e) MDCsRR at 5.4 GHz and (f) MDCsRR at 5.8 GHz.

where $\varepsilon_{eff} = \frac{\varepsilon_r+1}{2} + \frac{\varepsilon_r-1}{2}\frac{1}{\sqrt{1+12\frac{h}{w}}}$.

First resonance in the proposed antenna is due to central left and right sided highest surface current distribution on inter digital capacitor finger (Figure 9(a)). At resonance this length should be half wavelength in medium. Approximate radiating elements length responsible for first resonance can be calculated by using geometrical dimensions given in Table 2.

Table 2. Measured and simulated frequency bands of prototype antenna.

Band	Simulated Frequency Band (GHz)	Simulated BW (MHz)	Measured Frequency Band (GHz)	Measured BW (MHz)
First	3.16 to 3.25	90	3.17 to 3.25	80
Second	5.37 to 5.43	60	5.37 to 5.43	60
Third	5.77 to 5.85	80	5.75 to 5.87	120

Resonating length can be calculated as

$$L_{r_1} = L_i + W_i + \frac{L_i}{2} + \frac{L_i}{2} + G_i + L_i \tag{5}$$

By using Table 2, $L_{r1} = 29.80$ mm. The effective dielectric constant (ε_{reff}) is 2.092, calculated by equations given in [12]. At resonance L_{r1} should be $\lambda_g/2$, and the resonant frequency f_{r1} is given as $f_{r1} = \frac{c}{2L_{r1}\sqrt{\varepsilon_{reff}}} \approx 3.48$ GHz. Error generated due to this validation approach is 8%.

Second resonance band is generated due to left and right sided surface current distribution on interdigital capacitor (Figure 9(b)). Approximate length of radiating patch element at this frequency can be calculated as

$$L_{r2} = \frac{L_i}{2} + G_i + \frac{L_i}{2} + \frac{L_i}{2} + \frac{L_i}{2} + G_i \tag{6}$$

By using Table 2, $L_{r2} = 19.20\,\text{mm}$ and at resonance L_{r2} should be $\lambda_g/2$, and the resonant frequency f_{r2} is given as $f_{r2} = \frac{c}{2L_{r2}\sqrt{\varepsilon_{reff}}} \approx 5.40\,\text{GHz}$. Error generated due to this validation approach is 1.3%.

The electrical length contributing to third resonance band (Figure 9(c)) is given as

$$L_{r3} = \frac{L_i}{4} + \frac{L_i}{4} + G_i + L_i + \frac{L_i}{2} \tag{7}$$

By using Table 2, $L_{r3} = 18.20\,\text{mm}$ and at resonance L_{r3} should be $\lambda_g/2$, and the resonant frequency f_{r3} is given as $f_{r3} = \frac{c}{2L_{r3}\sqrt{\varepsilon_{reff}}} \approx 5.69\,\text{GHz}$. Error generated due to this validation approach is 2.7%.

The surface current distribution plot indicates maxima of current on interdigital capacitor finger and MDCsRR in the ground plane. Figure 10(a) shows the effect of variation of finger length of interdigital capacitor. Interdigital capacitor finger length "L_i" is changed from 8.00 mm to 9.50 mm. As length of the finger increases equivalent capacitance "C_{eq}" also increases causing resonant frequency "f_o" to decrease as in Figure 10(a).

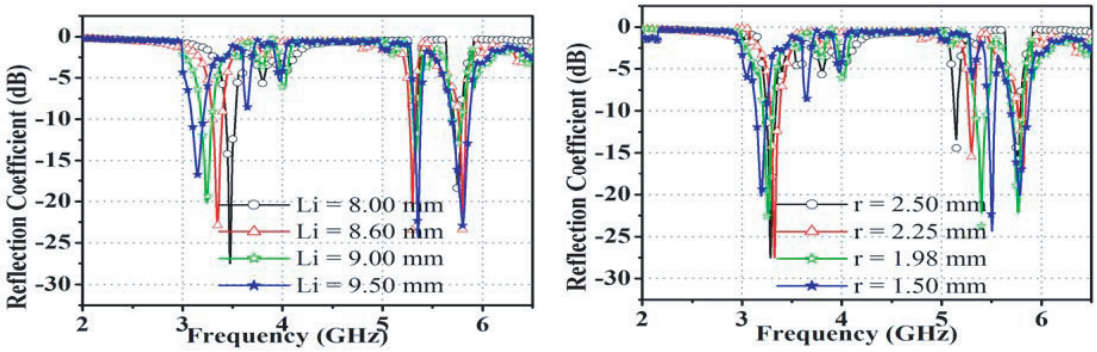

Figure 10. Reflection coefficient versus frequency for (a) various values of finger length of IDC — "Li" and (b) various values of radius of inner circular slot ring resonator of MDCsRR — "r".

At the second and third resonant bands, surface current is on some part of the interdigital capacitor, but the main highest current distribution is observed on MDCsRR in the ground plane. For second resonance band, surface current distribution maxima is mainly concentrated on inner circular slot ring resonator (CsRR) as shown in Figure 9(e). Figure 10(b) shows effect of variation of radius of inner CsRR on return loss. The radius of inner CsRR "r" is changed from 2.50 mm to 1.50 mm. As "r" decreases, equivalent inductance "L_{eq}" and equivalent capacitance "C_{eq}" decrease causing increase in the resonant frequency "f_o" as shown in Figure 10(b).

At the third resonant frequency surface current distribution maxima is mainly concentrated on outer CsRR as shown in Figure 9(f). Figure 11 shows effect of variation of radius of outer CsRR. As

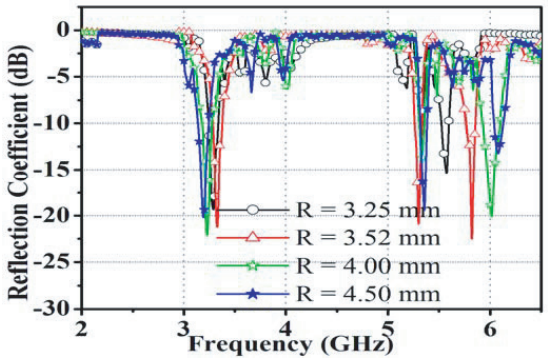

Figure 11. Reflection coefficient versus frequency for various values of radius of outer circular slot ring resonator of MDCsRR — "R".

"R" increases equivalent inductance "L_{eq}" and equivalent capacitance "C_{eq}" decrease causing increase in the resonant frequency "f_o" as shown in Figure 11. The effect of change in metallic strip thickness of MDCsRR "t" is also studied. No significant change in any of the resonant band frequencies is observed. It is also observed that we can independently control each of the resonant frequencies.

3. FABRICATED ANTENNA AND THE MEASUREMENT

The proposed patch antenna has electrical size of $0.20\lambda \times 0.20\lambda \times 0.008\lambda$ (19 mm × 19 mm × 0.762 mm) where λ is associated with first resonance frequency 3.2 GHz. Conventional patch antenna size operating at 3.2 GHz (31.25 mm × 37.05 mm × 0.762 mm) is miniaturized by 68.83%. The loading of IDC patch antenna with new metamaterial unit cell causes electrical size reduction as well as multi-band operation with significant calculated antenna gain. The top and back views of the fabricated prototype are shown in Figure 12(a) and Figure 12(b), respectively.

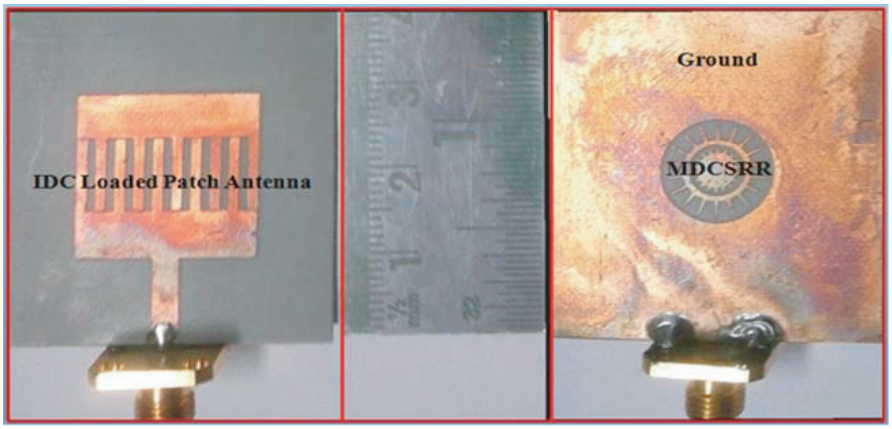

(a) (b)

Figure 12. Fabricated MDCsRR metamaterial unit cell loaded microstrip patch antenna. (a) Top View and (b) back View.

The measured and simulated return losses (S_{11}) of the prototype antenna loaded with MDCsRR metamaterial unit cell show good agreement as seen from Figure 13. The measured and simulated 10 dB return loss bandwidths for all the three bands are given in Table 2.

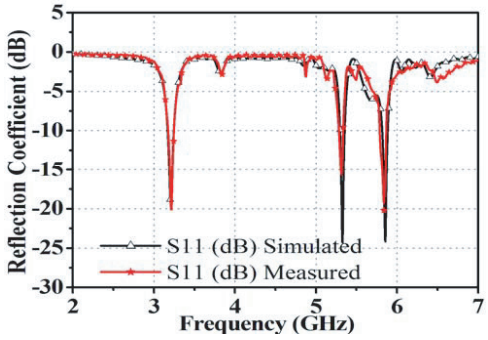

Figure 13. Simulated and measured reflection coefficient (S_{11}) of the prototype antenna.

The radiation pattern of the fabricated antenna is measured in an anechoic chamber using spectrum analyzer and signal generator. Figure 14 shows the measured and simulated E- and H-plane radiation patterns which demonstrate good agreement except small mismatch in E-plane radiation pattern at 5.4 GHz. The radiation pattern of the antenna with vertical linear electrical field polarization is similar

to a short monopole on a finite ground plane. The antenna has a both sided radiation pattern due to etched MDCsRR in the ground plane. The back radiation is less than the forward radiation due to the effect of finite ground plane used. Hence the proposed antenna has both sided radiation characteristics with higher gain in broad side and medium gain in back side. There is good cross polarization purity at the first resonating frequency of 3.2 GHz with a maximum measured electric field cross polarization level of −16.0 dB in E-plane and −12.23 dB cross polarization level in H-plane. The second band at resonant frequency of 5.4 GHz has maximum measured E-plane cross polarization level of −12.26 dB and H-plane cross polarization level of −14.21 dB. The third band with resonant frequency of 5.8 GHz has measured cross polarization level of −13.38 dB in H-plane and −22.11 dB in E-plane. The measured gain of the fabricated prototype antenna as a function of frequency is plotted in Figure 15. The measured gain plot indicates significant measured gain in all the three bands with maximum measured gain of 3.28 dBi at the first resonant frequency of 3.2 GHz. The second band with resonating frequency of 5.4 GHz and third band with resonating frequency of 5.8 GHz have 2.76 dBi and 3.1 dBi measured gains, respectively. The above measured gains are in broad side direction ($\theta = 0°$). The back side ($\theta = 180°$) gain of

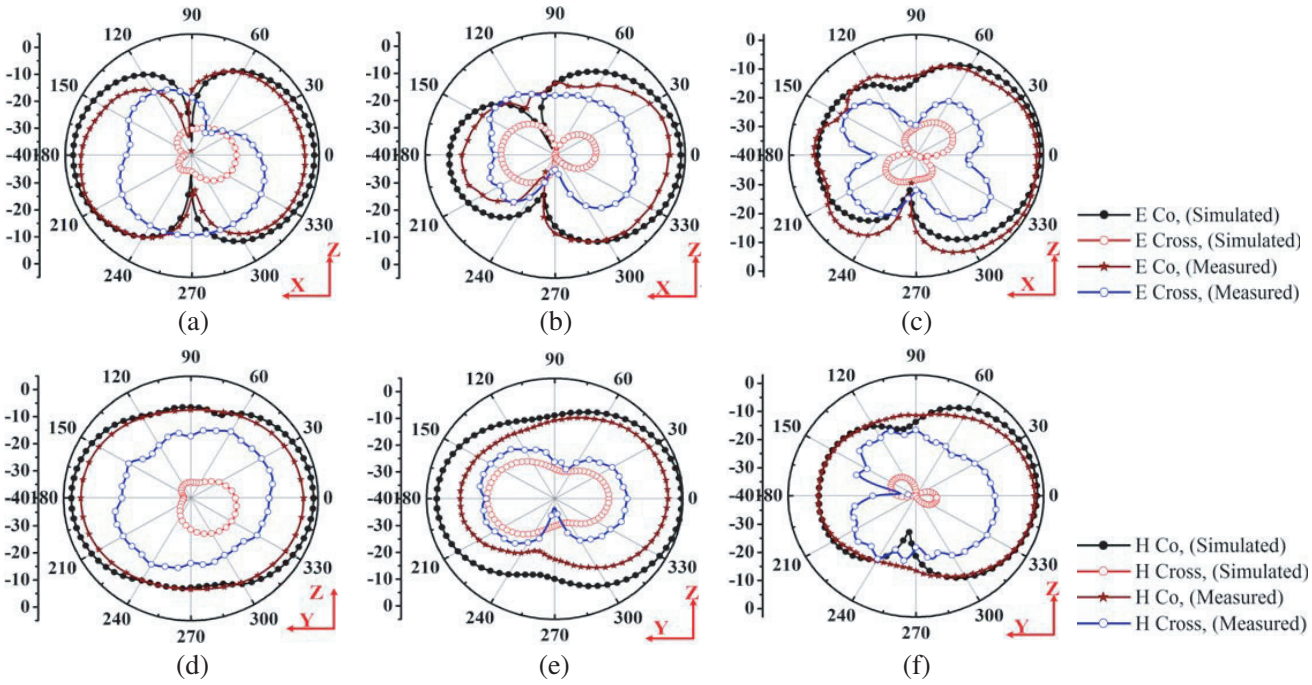

Figure 14. Radiation pattern of proposed antenna. (a) E Plane at 3.2 GHz. (b) E Plane at 5.4 GHz. (c) E Plane at 5.8 GHz. (d) H Plane at 3.2 GHz. (e) H Plane at 5.4 GHz and (f) H plane at 5.8 GHz.

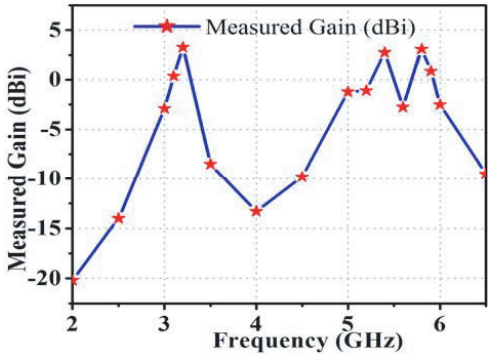

Figure 15. Measured gain versus frequency plot of the prototype antenna.

proposed antenna is also realized and found to be 2.1 dBi, 0.75 dBi and 1.3 dBi for the first, second and third resonant frequencies, respectively. The measured gain of the patch antenna in both sides ($\theta = 0°$ and $\theta = 180°$) is significantly high in all the three bands in spite of small electrical size of the proposed patch antenna. Hence, the proposed antenna is a double sided radiating patch antenna.

Table 3 compares the performance of different multi-band antennas reported with the proposed antenna. As observed, the proposed antenna has the smallest size with controlled triple band operation and offers the highest measured broad side and back side antenna gains with 68.83% miniaturization as compared to other reported antennas.

Table 3. Comparison of proposed antenna with other reported antennas.

Ref.	Size in terms of λ (Wavelength at lowest resonant frequency) $X \times Y \times Z$	Frequency Band (GHz)	Calculated Gain (dBi)
7	$0.260 \times 0.355 \times 0.018$	3.55, 5.55	1.12, 0.8
8	$0.204 \times 0.250 \times 0.006$	2.4, 5.2, 5.8	0.4, 1.6, 3.5
11	$0.191 \times 0.038 \times 0.003$	1.15, 2.88, 3.72	0.11, 3.26, 2.90
13	$0.158 \times 0.208 \times 0.013$	2.5, 3.5, 5.5	1.5, 1.7, 3.05
14	$0.099 \times 0.149 \times 0.038$	2.4, 5.0	2.1, 5.3
15	$0.199 \times 0.199 \times 0.008$	3.15, 5.28	2.84, 3.86
17	$0.15 \times 0.15 \times 0.01$	2.6, 3.47, 5.75	0.2, 0.16, 0.62
18	$0.13 \times 0.13 \times 0.016$	2.59, 4.73, 5.7	2.59, 3.58, 2.29
Proposed	$0.202 \times 0.202 \times 0.008$	3.2, 5.4, 5.8	3.28, 2.76, 3.1

4. CONCLUSIONS

A highly miniaturized significant gain triple band patch antenna loaded with a new modified double circular slot ring resonator (MDCsRR) metamaterial unit cell is successfully demonstrated. The proposed antenna size is miniaturized by about 68.83% as compared to a conventional patch antenna size (31.25 mm × 37.05 mm × 0.762 mm) operating at the first resonant frequency of 3.2 GHz with significant calculated antenna gain at all the three bands. As a tradeoff, increased level of miniaturization causes reduction in −10 dB reflection coefficient bandwidth with good radiation pattern in broad side and back side directions. The transmission line model of MDCsRR and IDC loaded patch antenna is presented and fabricated, showing passband characteristic at all the resonating bands. IDC and MDCsRR add finite capacitance and inductance to the equivalent patch antenna circuit, causing increase in series capacitance and hence reduction in electrical size of the antenna. Multiband operation is achieved by multimode propagation due to MDCsRR and IDC. The proposed antenna has wide range applications in WiMax and WLAN bands.

REFERENCES

1. Caloz, C., T. Itoh, and A. Rennings, "CRLH metamaterial leaky-wave and resonant antennas," *IEEE Antennas and Propagation Magazine*, Vol. 50, No. 5, 25–39, Oct. 2008.
2. Ouedraogo, R. O., E. J. Rothwell, A. R. Diaz, K. Fuchi, and A. Temme, "Miniaturization of patch antennas using a metamaterial-inspired technique," *IEEE Transactions on Antennas and Propagation*, Vol. 60, No. 5, 2175–2182, May 2012.
3. Dong, Y., H. Toyao, and T. Itoh, "Design and characterization of miniaturized patch antennas loaded with complementary split-ring resonators," *IEEE Transactions on Antennas and Propagation*, Vol. 60, No. 2, 772–785, Feb. 2012.
4. Lee, Y., S. Tse, Y. Hao, and C. G. Parini, "A compact microstrip antenna with improved bandwidth using Complementary Split-Ring Resonator (CSRR) loading," *2007 IEEE Antennas and Propagation Society International Symposium*, 5431–5434, Honolulu, HI, 2007.

5. Xie, Y., L. Li, C. Zhu, and C.-H. Liang, "A novel dual-band patch antenna with complementary split ring resonators embedded in the ground plane," *Progress In Electromagnetics Research Letters*, Vol. 25, 117–126, 2011.
6. Ha, J., K. Kwon, Y. Lee, and J. Choi, "Hybrid mode wideband patch antenna loaded with a planar metamaterial unit cell," *IEEE Transactions on Antennas and Propagation*, Vol. 60, No. 2, 1143–1147, Feb. 2012.
7. Antoniades, M. A. and G. V. Eleftheriades, "A broadband dual-mode monopole antenna using NRI-TL metamaterial loading," *IEEE Antennas and Wireless Propagation Letters*, Vol. 8, 258–261, 2009.
8. Si, L.-M. and X. Lv, "CPW-fed multi-band omni-directional planar microstrip antenna using composite metamaterial resonators for wireless communications," *Progress In Electromagnetics Research*, Vol. 83, 133–146, 2008.
9. Ziolkowski, R. W., P. Jin, and C. C. Lin, "Metamaterial-inspired engineering of antennas," *Proceedings of the IEEE*, Vol. 99, No. 10, 1720–1731, Oct. 2011.
10. Zhu, J. and G. V. Eleftheriades, "Dual-band metamaterial-inspired small monopole antenna for WiFi applications," *Electronics Letters*, Vol. 45, No. 22, 1104–1106, Oct. 22, 2009.
11. Antoniades, M. A. and G. V. Eleftheriades, "Multiband compact printed dipole antennas using NRI-TL metamaterial loading," *IEEE Transactions on Antennas and Propagation*, Vol. 60, No. 12, 5613–5626, Dec. 2012.
12. Balanis, C. A., *Antenna Theory Analysis and Design*, 3rd Edition, Wiley, Hoboken, NJ, USA, 2005.
13. Gautam, A. K., L. Kumar, B. K. Kanaujia, and K. Rambabu, "Design of compact F-shaped slot triple-band antenna for WLAN/WiMAX applications," *IEEE Transactions on Antennas and Propagation*, Vol. 64, No. 3, 1101–1105, Mar. 2016.
14. Brocker, D. E., Z. H. Jiang, M. D. Gregory, and D. H. Werner, "Miniaturized dual-band folded patch antenna with independent band control utilizing an interdigitated slot loading," *IEEE Transactions on Antennas and Propagation*, Vol. 65, No. 1, 380–384, Jan. 2017.
15. Singh, A. K., M. P. Abegaonkar, and S. K. Koul, "Highly miniaturized dual band patch antenna loaded with metamaterial unit cell," *Microwave and Optical Technology Letters*, Vol. 59, No. 8, 2027–2033, May 2017.
16. Kurra, L., M. P. Abegaonkar, and S. K. Koul, "Equivalent circuit model of resonant EBG band stop filter," *IETE Journal of Research*, Vol. 62, No. 1, 17–26, Jan. 2016.
17. Ali, T. and R. C. Biradar, "A triple band highly miniaturized antenna for WiMAX/WLAN applications," *Microwave and Optical Technology Letters*, Vol. 60, 466–471, 2018.
18. Boukarkar, A., X. Q. Lin, Y. Jiang, and Y. Q. Yu, "Miniaturized single-feed multiband patch antennas," *IEEE Transactions on Antennas and Propagation*, Vol. 65, No. 2, 850–854, Feb. 2017.
19. Kumar, A., M. P. Abegaonkar, and S. K. Koul, "Triple band miniaturized patch antenna loaded with metamaterial unit cell for defense applications," *2016 11th International Conference on Industrial and Information Systems (ICIIS)*, 833–837, Roorkee, 2016.
20. Rahimi, M., F. B. Zarrabi, R. Ahmadian, Z. Mansouri, and A. Keshtkar, "Miniaturization of antenna for wireless application with difference metamaterial structures," *Progress In Electromagnetics Research*, Vol. 145, 19–29, 2014.
21. Sharma, S. K., A. Gupta, and R. K. Chaudhary, "Epsilon negative CPW-fed zeroth-order resonating antenna with backed ground plane for extended bandwidth and miniaturization," *IEEE Transactions on Antennas and Propagation*, Vol. 63, No. 11, 5197–5203, Nov. 2015.
22. Gupta, A., S. K. Sharma, and R. K. Chaudhary, "A compact dual-mode metamaterial-inspired antenna using rectangular type CSRR," *Progress In Electromagnetics Research*, Vol. 57, 35–42, 2015.
23. Sharma, S. K., M. A. Abdalla, and R. K. Chaudhary, "An electrically small SICRR metamaterial-inspired dual-band antenna for WLAN and WiMAX applications," *Microwave and Optical Technology Letters*, Vol. 59, No. 3, 573–578, 2017.